THE JOURNAL OF PHYSICAL CHEMISTRY Letters

Letter

pubs.acs.org/JPCL

Formation of High-Aspect-Ratio Helical Nanorods via Chiral Self-Assembly of Fullerodendrimers

Andrew J. Hilmer,[†,⊥] Darin O. Bellisario,[†,§] Steven Shimizu,[†] Thomas P. McNicholas,[†] Qing Hua Wang,[†] Scott A. Speakman,[‡] and Michael S. Strano*[,†]

[†]Department of Chemical Engineering, [§]Department of Chemistry, and [‡]Center for Materials Science and Engineering, Massachusetts Institute of Technology, Cambridge, Massachusetts 02139, United States

Supporting Information

ABSTRACT: Two novel, asymmetric methanofullerenes are presented, which self-assemble in cyclohexane upon thermal cycling to 80 °C. We show that, through the introduction of a dipeptide sequence to one terminus of the dendritic methanofullerene, it is possible to transform the assembly behavior of these molecules from poorly formed aggregates to high-aspect-ratio nanorods. These nanorods have diameters of 3.76 ± 0.52 nm and appear to be composed of interwoven helices of dendritic fullerenes. As evidenced by circular dichroism, the helicity is characterized by a preferential handedness of assembly, which is imparted by the dipeptide moiety.

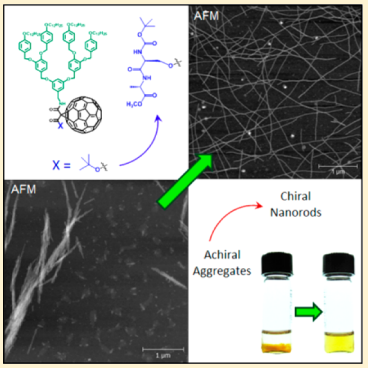

SECTION: Glasses, Colloids, Polymers, and Soft Matter

The ability to form well-defined fullerene nanostructures via self-assembly is desirable for applications in polymer photovoltaics and organic electronics.[1−4] Fullerenes are excellent electron acceptors,[5] and in organic photovoltaics, they have remained the electron acceptor of choice since their usage in the first bulk heterojunction photovoltaic in the mid-1990s.[6] The need to control the assembly and morphology of fullerenes is featured prominently in the organic electronic literature. For example, high photoconversion efficiency in organic photovoltaics is dependent upon fullerene dispersion within the active layer.[7,8] In addition, structured arrays of C_{60} fullerenes have been shown to possess highly delocalized electronic states,[9,10] and superconducting properties have been observed in intercalated C_{60} networks.[11−13] Hence, for such applications, it is highly desirable to be able to control the assembly and patterning of fullerene molecules.

Only a few instances of nanometer-scale, high-aspect-ratio fullerene assembles have been reported, and these have relied on surface-based assembly methods,[14−17] including Langmuir−Blodgett techniques,[14] or HOPG-driven self-assembly,[15,16] thereby limiting their scalability. In contrast, the assembly of fullerenes on larger length scales has been accomplished through a number of methods,[1] including liquid−liquid interfacial precipitation (LLIP), template-assisted drying, and drop drying. In addition to these, functionalized fullerenes have been shown to form a variety of bilayer structures, depending upon solvent conditions and chemical derivatization.[18] However, the dimensions of these assemblies (typically on the order of several hundred nanometers to a few micrometers) are too large for many organic electronics applications. In addition to approaches based on self-assembly, a variety of fullerene polymers have been synthesized.[19] However, in these cases, the physical constraints of the polymer backbone may impose limits on the extent of interfullerene interaction.

In biologically inspired self-assembly, di- and tripeptide conjugates have been shown to act as low-molecular-weight hydrogelators,[20] and the ability of polypeptides to form self-assembled nanostructures has been extensively studied.[21] Recently, it was demonstrated that dendritic dipeptides could self-assemble into cylindrical nanopores and enable the transport of protons through liposomes.[22] Building on these studies, we sought to determine the influence of dipeptide incorporation on the assembly of dendritic methanofullerenes.

We report the synthesis of a novel pair of fullerodendrimers (Figure 1), which self-assemble into one-dimensional fibers in cyclohexane. We find that high-aspect-ratio fullerene nanorods, with diameters of 3.76 ± 0.52 nm, can be formed by utilizing peptide-driven self-assembly. These structures appear to consist of interwoven, helical assemblies of peptidic methanofullerenes.

In order to construct these molecules, second-generation benzyl dendrons of the form [4−3,4−3,5]12G_2CH_2CN were generally synthesized according to the scheme of Percec et al.,[22] with the only exception being the use of 3,5-dihydroxybenzonitrile in the formation of the second-generation apex, thereby

Received: January 22, 2014
Accepted: February 14, 2014

   dx.doi.org/10.1021/jz500138d | J. Phys. Chem. Lett. 2014, 5, 929−934

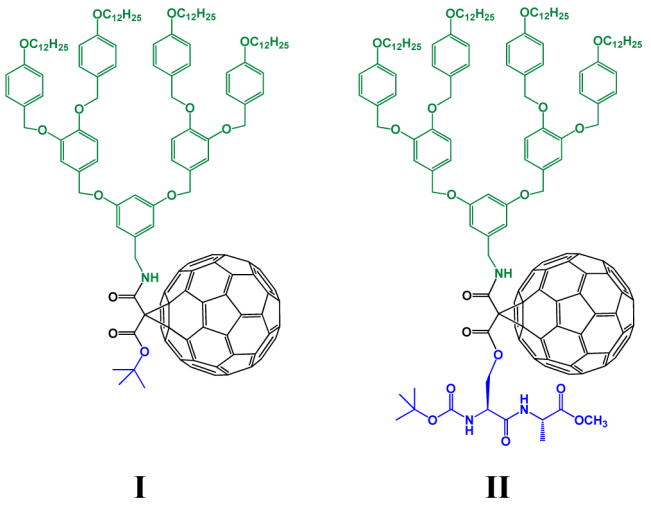

Figure 1. Molecular structures of the fullerodendrimers studied in this work.

allowing for the introduction of an amine functionality at this terminus. Treatment of the cyano adduct with $LiAlH_4$ gave the primary amine, $[4-3,4-3,5]12G_2CH_2NH_2$. Reaction of the aminated second-generation dendron with mono-*tert*-butyl malonate via DCC/DMAP coupling yielded the dendritic precursor to **I**, which was then conjugated to C_{60} fullerene by Bingel addition.[23] For the formation of **II**, the aminated second-generation dendron was coupled to methyl-3-chloro-3-oxopropionate, after which the methyl ester was cleaved under basic conditions,[24] thereby allowing for the conjugation of the dipeptide sequence, Boc-L-Ser-L-Ala-OMe. This intermediate was coupled to C_{60} using Bingel conditions to yield fullerodendrimer **II**.

While fullerodendrimers **I** and **II** are structurally similar, they display substantially different assembly behavior in the solution phase. This was first evidenced by their disparate behavior in variable-temperature absorbance measurements. Upon heating, both molecules could be dissolved in cyclohexane to yield homogeneous light-yellow to light-red solutions at 75−80 °C. Figure 2 shows temperature-dependent absorbance results for the two fullerodendrimers. Upon cooling, the fullerene absorbance feature at 259 nm undergoes a decrease, while there is an increase in a red-shifted absorbance feature at approximately 267 nm. The emergent feature is broader in the case of fullerodendrimer **I**, likely indicating a greater degree of inhomogeneity in the structure of the formed assemblies, which is in agreement with morphological results, discussed below. In addition, the assembly transition of the two molecules occurs at different temperatures for the two species (Figure 2c), with an onset of assembly at around 50 °C for the dipeptide derivative and an assembly onset of approximately 30 °C for the *t*-butyl derivative. These differences in temperature-dependent assembly can be qualitatively observed during the simultaneous cooling of solutions of fullerodendrimers **I** and **II** from an isotropic state, during which the dipeptide derivative transitions to a deep-yellow color earlier in the cooling process (Figure S1, Supporting Information). In addition, upon sitting for 24 h, fullerodendrimer **II** remains dispersed, while its peptide-free analogue sediments out of solution (Figure S1, Supporting Information). Together, these results indicate that there are differences in the assembled structures formed by these two molecules and that the dipeptide moiety plays an integral role in the assembly of fullerodendrimer **II**.

We hypothesize that the first step in the assembly process involves a wrapping of the fullerene moiety by the benzyl ether dendron, resulting in an initial, gradual increase in the absorbance feature at 259 nm. In the absence of the dipeptide, these complexes are stable to approximately 30 °C, at which point nonspecific aggregation occurs. In the presence of the dipeptide, the onset of intermolecular hydrogen bonding drives the assembly of the fullerodendrimer at a much higher temperature. Solution-phase assembly is further supported by variable-temperature ^1H NMR experiments, which show a broadening and decrease in proton signal intensities upon cooling, until the only observable signal is that attributable to the terminal, aliphatic chains of the dendron (Supporting Information).

Differences in assembly behavior were further observed through morphological analysis of the suspensions. Figure 3a and d show SEM images of drop-dried solutions of the *t*-butyl and dipeptide derivatives, respectively. Here, it is evident that the dipeptide derivative forms high-aspect-ratio fibers, which

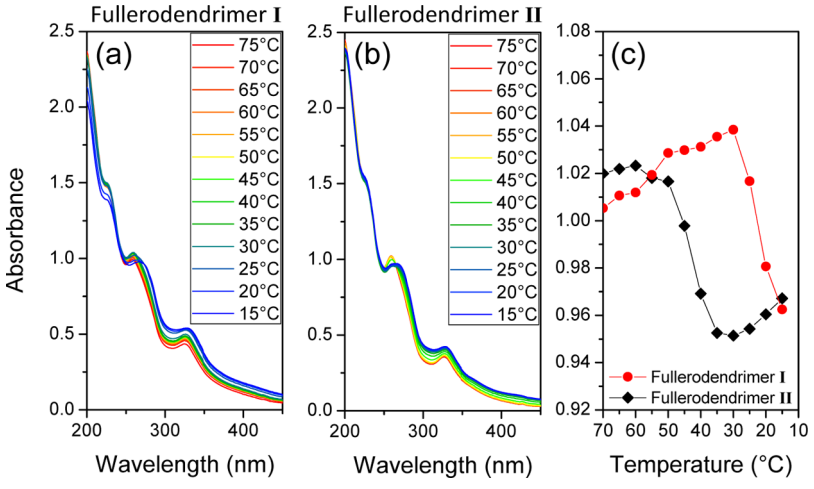

Figure 2. Temperature-dependent absorbance data for (a) fullerodendrimer I and (b) fullerodendrimer **II** in cyclohexane at a concentration of 78 μM. (c) Absorbance at 259 nm as a function of temperature. Upon cooling from an isotropic state, the fullerene peak at 259 nm decreases, with the evolution of a new peak near 267 nm. The transition temperature occurs approximately 20 °C higher in the case of fullerodendrimer **II**.

dx.doi.org/10.1021/jz500138d | *J. Phys. Chem. Lett.* 2014, 5, 929−934

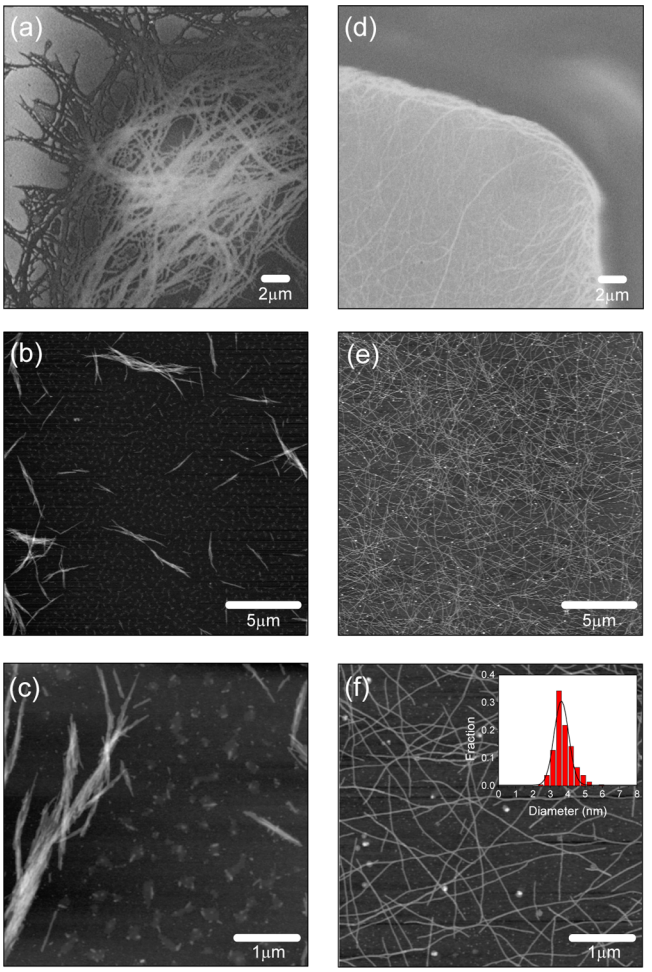

Figure 3. SEM (a,d) and AFM (b,c,e,f) images of self-assembled morphology. (d) SEM of a drop-cast solution of **II** shows the formation of densely matted regions of aligned fibers, while (a) SEM of a drop-cast solution of **I** shows randomly oriented domains. (e,f) AFM on spin-cast assemblies of **II** show structurally homogeneous fibers with average diameters of 3.76 ± 0.52 nm and lengths of a few hundred nanometers to >10 μm. (b,c) AFM on spin-cast assemblies of **I** show the formation of aggregated fibers, rather than well-formed nanorods.

pack into densely matted regions in the solid state. In contrast, the *t*-butyl derivative shows a less-ordered assembly behavior, which prohibits the formation of dense regions. These results are confirmed by AFM. Here, it is observed that the dipeptide derivative forms self-assembled wires with diameters of 3.76 ± 0.52 nm and lengths that can exceed 10 μm. In contrast, the *t*-butyl derivative forms poorly assembled fibers, which further aggregate into larger assemblies.

Interestingly, the morphology of the peptidic nanowires changes over time. Upon standing for several weeks, AFM reveals that the initial, straight fullerene wires transform into a combination of straight wires and spiral assemblies, with clear junctions between the two types of structures. AFM phase and height images of these helical assemblies are presented in Figure 4. As can be seen from the height traces in Figure 4b, the peaks of these helices occur at heights close to 3.5 nm, which is consistent with the diameter distribution of the initial, straight fullerene wires. In contrast, the valleys along the helix possess heights of approximately half of this value. These results seem to indicate that the initially formed fullerene wires consist of

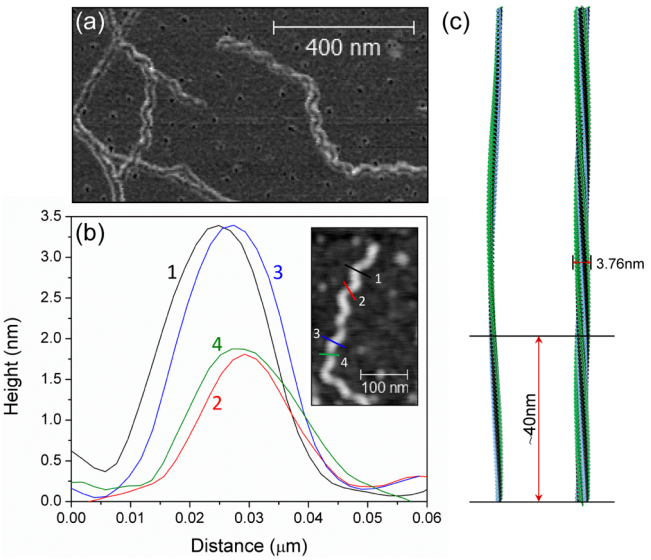

Figure 4. AFM (a) phase image and (b) height profiles obtained from unraveled helical assemblies of fullerodendrimer **II**. The inset of (b) shows a height image of an isolated, helical fiber, along with the positions at which height traces were evaluated. In these unraveled fibers, peak values near 3.4 nm are in close agreement with the diameter of the full nanorods, while valley heights (~1.8 nm) are approximately one-half of the diameter of the full fibers. (c) Hypothesized schematic of the assembly. The full nanorods (right) appear to be composed of multiple interwoven helical fibers. A single, helical fiber is shown on the left. The axial wrapping periodicity of the full nanorods is 40 ± 4 nm (further discussed below).

multiple interwoven strands of fullerodendrimer **II**, which can unravel over time. Such a structure is depicted in Figure 4c. This is further supported by the observation of helical striations in AFM phase images of intact fullerene nanorods (Figure 5). From these images, the helical pitch of these assemblies appears to be approximately 40 ± 4 nm.

We attempted to obtain periodicity information by performing grazing-incidence small-angle X-ray scattering (GI-SAXS) measurements on drop-dried films of fullerodendrimers **I** and **II**. However, film-to-film variations in scattering results seemed to indicate that the observed scattering features were primarily

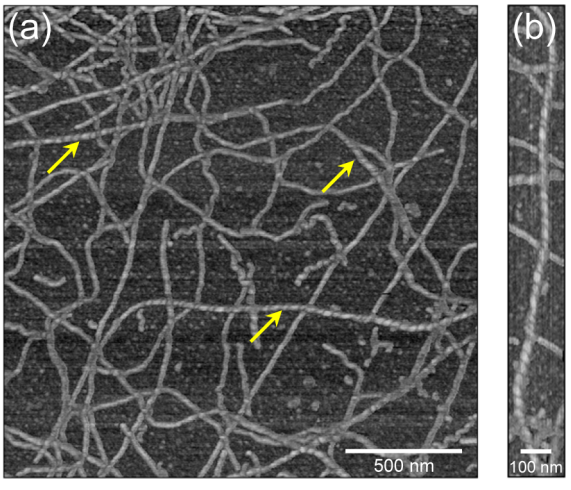

Figure 5. AFM phase images of assembled fullerodendrimer **II** showing helical striations along the length of the assembled nanorods. (b) Zoomed-in phase image of one of these assemblies.

dx.doi.org/10.1021/jz500138d | *J. Phys. Chem. Lett.* 2014, 5, 929−934

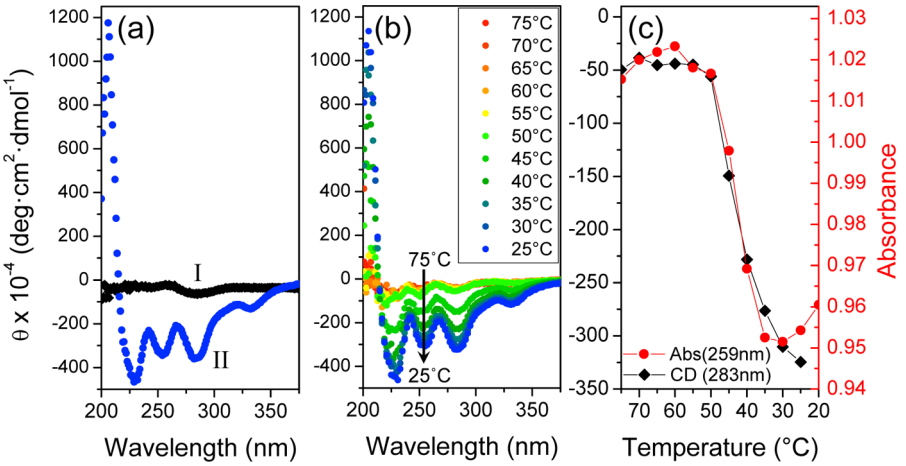

Figure 6. (a) Room-temperature CD spectra of fullerodendrimers **I** and **II**. Fullerodendrimer **I**, which lacks the dipeptide sequence, shows no significant CD features, whereas fullerodendrimer **II** shows clear spectral features, indicating selectivity toward a particular handedness during self-assembly. (b) Supramolecular CD features emerge upon cooling of fullerodendrimer **II** from an isotropic state. (c) Comparison between temperature-dependent absorbance (259 nm) and the temperature-dependent CD signal at 283 nm.

attributable to the morphology of the films, rather than the nanorod periodicity of assembly (Figures S5 and S6, Supporting Information).

The direct observation of helicity in these structures by AFM led us to question whether a racemic mixture of left- and right-handed assemblies is formed or if the chirality of the peptide drives the selective formation of a particular supramolecular structure. To examine this, we conducted circular dichroism (CD) measurements on the two fullerodendrimers. The results of CD measurements are shown in Figure 6. In Figure 6c, we show room-temperature CD spectra for both fullerodendrimers **I** and **II**. From these spectra, two properties of the assembly can be deduced. The first is that the self-assembly of fullerodendrimer **II** favors a particular handedness of helical arrangement. In combination with AFM results, it appears that left-handed helices are selectively formed in this system. In addition, the lack of CD features in the case of fullerodendrimer **I** indicates that the dipeptide molecule plays an integral role in the handedness of the resulting nanorod, as expected.

In addition to room-temperature measurements, variable-temperature CD spectra were acquired for fullerodendrimer **II** (Figure 6b). Upon heating the assembled molecules to an isotropic state, no significant CD features are observed. However, these features reappear upon cooling of the sample to room temperature. These results indicate that it is not the chirality of the molecule itself that imparts the CD signal but the handedness of the supramolecular assembly. In Figure 6c, we plot the change in CD signal at 289 nm as a function of temperature and overlay the response with that observed during variable-temperature absorbance measurements, finding very good agreement between these two experimental measurements. This result indicates that upon the initiation of self-assembly, near 50 °C, the helical sense of the nanorod is simultaneously specified by the stereochemistry of the dipeptide. Therefore, we anticipate the ability to readily tune the handedness of the nanorods by altering the chirality of this dipeptide, as has been demonstrated in similar systems.[25]

While the peptide appears to impart a handedness to the assembly, the methanofullerene is likely to play a stabilizing role. In studies employing dendritic dipeptides, it has been shown that the chemical nature of the amino acids[26] and peptide protective groups[27] can be altered to modulate the stability of the resulting supramolecular complex, as indicated by changes in the melting temperature of the complex in solution (T_m). In the case of fullerodendrimer **II**, a T_m of 43 °C is calculated at a solution concentration of 78 μM, based upon the transition midpoint in the variable-temperature CD spectra. This is 21 °C higher than the T_m of dendritic dipeptides that have employed similar protecting groups at a higher molecular concentration of 120 μM[22] (T_m increases with increasing concentration). This increased value of T_m in the case of the methanofullerene derivative seems to indicate that this additional hydrophobic group has a stabilizing effect on the resulting nanorods, which is consistent with prior observations that hydrophobic amino acids can increase the stability of self-assembled nanopores.[26]

In order to examine the electronic properties of these materials, we tested the self-assembled nanorods for electrical conductivity. Freshly prepared nanorod assemblies were deposited by spin-coating onto 6 μm wide Au electrodes, which were fabricated by electron beam lithography (EBL). The electrodes, which we call the source and drain, were separated by less than 100 nm on a substrate of 300 nm SiO_2/p-Si to back gate. For nanorod deposition, a 78 μM solution of fullerodendrimer **II** was first diluted to ~16 μM in cyclohexane, resulting in approximately 30 nanorods bridging the electrodes. The sample was then dried under nitrogen for 24 h to evaporate any retained solvent before electrically contacting with grounded electrodes at room temperature under sub-10^{-5} mbar vacuum. However, checking for conductivity using a source-drain voltage ranging from 10 mV to 10 V, and a back-gate bias of ±20 V, yielded no measurable current (<0.1 pA) for any of the 20 devices that were examined (see the Supporting Information for device images).

We also tested the electrical conductivity of the nanorods by conductive atomic force microscopy (cAFM). For current imaging, freshly prepared assemblies of fullerodendrimer **II** were spin-coated onto conductive indium tin oxide (ITO)-coated glass substrates. However, the simultaneous topographic and current images only showed conduction through the ITO substrate, with the fullerene nanorods hindering electrical transport, thereby indicating little to no conductivity in the radial direction (see the Supporting Information for additional details and cAFM images). On the basis of these results, we

dx.doi.org/10.1021/jz500138d | J. Phys. Chem. Lett. 2014, 5, 929−934

hypothesize that the dendritic portion of the molecule may hinder electrical transport by physically inhibiting interfullerene interactions. Because the dipeptide segment appears to play a prominent role in self-assembly, we anticipate that it may be possible to develop dendron-free derivatives, such that this interference is minimized.

In conclusion, we have synthesized two novel, asymmetric fullerodendrimers and analyzed their self-assembly behavior. Through the introduction of a dipeptide sequence to one terminus of the dendritic methanofullerene, we show that it is possible to change the self-assembly behavior from the formation of poorly ordered aggregates to high-aspect-ratio nanorods. The formation of nanorods is driven by interactions between the dipeptide moieties, and this interaction simultaneously imparts helicity to the resulting supramolecular assembly. We were unable to observe electrical conductivity in these assemblies, and it is possible that the dendron physically inhibits electronic interaction between adjacent fullerenes. Because the peptide segment appears to drive self-assembly in these constructs, we hypothesize that it may be possible to develop peptide−fullerene constructs that self-assemble in the absence of the attached dendron, thereby minimizing this effect.

■ ASSOCIATED CONTENT

Supporting Information

Experimental methods, synthetic protocols, X-ray scattering data, and variable-temperature NMR. This material is available free of charge via the Internet at http://pubs.acs.org.

■ AUTHOR INFORMATION

Corresponding Author

*E-mail: strano@mit.edu.

Present Address

[⊥]A.J.H.: Departments of Chemistry and Chemical Engineering, Stanford University, Stanford, California 94305, United States.

Notes

The authors declare no competing financial interest.

■ ACKNOWLEDGMENTS

A.J.H. acknowledges funding from the Department of Energy Office of Science Graduate Fellowship Program (DOE SCGF), made possible in part by the American Recovery and Reinvestment Act of 2009, administered by ORISE-ORAU under Contract No. DE-AC05-06OR23100. D.O.B. acknowledges the Department of Defense for financial support.

■ REFERENCES

(1) Babu, S. S.; Mohwald, H.; Nakanishi, T. Recent Progress in Morphology Control of Supramolecular Fullerene Assemblies and Its Applications. *Chem. Soc. Rev.* **2010**, *39*, 4021−4035.

(2) Li, H.; Babu, S. S.; Turner, S. T.; Neher, D.; Hollamby, M. J.; Seki, T.; Yagai, S.; Deguchi, Y.; Mohwald, H.; Nakanishi, T. Alkylated-C_{60} Based Soft Materials: Regulation of Self-Assembly and Optoelectronic Properties by Chain Branching. *J. Mater. Chem. C* **2013**, *1*, 1943−1951.

(3) Mas-Torrent, M.; Rovira, C. Novel Small Molecules for Organic Field-Effect Transistors: Towards Processability and High Performance. *Chem. Soc. Rev.* **2008**, *37*, 827−838.

(4) Delgado, J. L.; Bouit, P.-A.; Filippone, S.; Herranz, M. a. A.; Martin, N. Organic Photovoltaics: A Chemical Approach. *Chem. Commun.* **2010**, *46*, 4853−4865.

(5) Liu, T.; Troisi, A. What Makes Fullerene Acceptors Special as Electron Acceptors in Organic Solar Cells and How to Replace Them. *Adv. Mater.* **2013**, *25*, 1038−1041.

(6) Yu, G.; Gao, J.; Hummelen, J. C.; Wudl, F.; Heeger, A. J. Polymer Photovoltaic Cells — Enhanced Efficiencies via a Network of Internal Donor−Acceptor Heterojunctions. *Science* **1995**, *270*, 1789−1791.

(7) Chen, W.; Nikiforov, M. P.; Darling, S. B. Morphology Characterization in Organic and Hybrid Solar Cells. *Energy Environ. Sci.* **2012**, *5*, 8045−8074.

(8) Yang, X.; Loos, J. Toward High-Performance Polymer Solar Cells: The Importance of Morphology Control. *Macromolecules* **2007**, *40*, 1353−1362.

(9) Feng, M.; Zhao, J.; Petek, H. Atomlike, Hollow-Core-Bound Molecular Orbitals of C_{60}. *Science* **2008**, *320*, 359−362.

(10) Zhao, J.; Feng, M.; Yang, J. L.; Petek, H. The Superatom States of Fullerenes and Their Hybridization into the Nearly Free Electron Bands of Fullerites. *ACS Nano* **2009**, *3*, 853−864.

(11) Ganin, A. Y.; Takabayashi, Y.; Jeglic, P.; Arcon, D.; Potocnik, A.; Baker, P. J.; Ohishi, Y.; McDonald, M. T.; Tzirakis, M. D.; McLennan, A.; Darling, G. R.; Takata, M.; Rosseinsky, M. J.; Prassides, K. Polymorphism Control of Superconductivity and Magnetism in Cs_3C_{60} Close to the Mott Transition. *Nature* **2010**, *466*, 221−225.

(12) Hebard, A. F.; Rosseinsky, M. J.; Haddon, R. C.; Murphy, D. W.; Glarum, S. H.; Palstra, T. T. M.; Ramirez, A. P.; Kortan, A. R. Superconductivity at 18 K in Potassium-Doped $C6_0$. *Nature* **1991**, *350*, 600−601.

(13) Tanigaki, K.; Ebbesen, T. W.; Saito, S.; Mizuki, J.; Tsai, J. S.; Kubo, Y.; Kuroshima, S. Superconductivity at 33 K in $Cs_xRb_yC_{60}$. *Nature* **1991**, *352*, 222−223.

(14) Tsunashima, R.; Noro, S. I.; Akutagawa, T.; Nakamura, T.; Kawakami, H.; Toma, K. Fullerene Nanowires: Self-Assembled Structures of a Low-Molecular-Weight Organogelator Fabricated by the Langmuir−Blodgett Method. *Chem.—Eur. J.* **2008**, *14*, 8169−8176.

(15) Muñoz, A.; Illescas, B. M.; Sánchez-Navarro, M.; Rojo, J.; Martín, N. Nanorods versus Nanovesicles from Amphiphilic Dendrofullerenes. *J. Am. Chem. Soc.* **2011**, *133*, 16758−16761.

(16) Nakanishi, T.; Miyashita, N.; Michinobu, T.; Wakayama, Y.; Tsuruoka, T.; Ariga, K.; Kurth, D. G. Perfectly Straight Nanowires of Fullerenes Bearing Long Alkyl Chains on Graphite. *J. Am. Chem. Soc.* **2006**, *128*, 6328−6329.

(17) Feng, M.; Lee, J.; Zhao, J.; Yates, J. T.; Petek, H. Nanoscale Templating of Close-Packed C_{60} Nanowires. *J. Am. Chem. Soc.* **2007**, *129*, 12394−12395.

(18) Nakanishi, T. Supramolecular Soft and Hard Materials Based on Self-Assembly Algorithms of Alkyl-Conjugated Fullerenes. *Chem. Commun.* **2010**, *46*, 3425−3436.

(19) Giacalone, F.; Martín, N. Fullerene Polymers: Synthesis and Properties. *Chem. Rev.* **2006**, *106*, 5136−5190.

(20) Adams, D. J. Dipeptide and Tripeptide Conjugates as Low-Molecular-Weight Hydrogelators. *Macromol. Biosci.* **2011**, *11*, 160−173.

(21) Liu, L.; Busuttil, K.; Zhang, S.; Yang, Y.; Wang, C.; Besenbacher, F.; Dong, M. The Role of Self-Assembling Polypeptides in Building Nanomaterials. *Phys. Chem. Chem. Phys.* **2011**, *13*, 17435−17444.

(22) Percec, V.; Dulcey, A. E.; Balagurusamy, V. S. K.; Miura, Y.; Smidrkal, J.; Peterca, M.; Nummelin, S.; Edlund, U.; Hudson, S. D.; Heiney, P. A.; Hu, D. A.; Magonov, S. N.; Vinogradov, S. A. Self-Assembly of Amphiphilic Dendritic Dipeptides into Helical Pores. *Nature* **2004**, *430*, 764−768.

(23) Bingel, C. Cyclopropanierung von Fullerenen. *Chem. Ber.* **1993**, *126*, 1957−1959.

(24) Percec, V.; Cho, W. D.; Ungar, G.; Yeardley, D. J. P. Synthesis and Structural Analysis of Two Constitutional Isomeric Libraries of AB_2-Based Monodendrons and Supramolecular Dendrimers. *J. Am. Chem. Soc.* **2001**, *123*, 1302−1315.

(25) Rosen, B. M.; Peterca, M.; Morimitsu, K.; Dulcey, A. E.; Leowanawat, P.; Resmerita, A. M.; Imam, M. R.; Percec, V. Programming the Supramolecular Helical Polymerization of Dendritic

Dipeptides via the Stereochemical Information of the Dipeptide. *J. Am. Chem. Soc.* **2011**, *133*, 5135−5151.
(26) Percec, V.; Dulcey, A. E.; Peterca, M.; Adelman, P.; Samant, R.; Balagurusamy, V. S. K.; Heiney, P. A. Helical Pores Self-Assembled from Homochiral Dendritic Dipeptides Based on l-Tyr and Nonpolar α-Amino Acids. *J. Am. Chem. Soc.* **2007**, *129*, 5992−6002.
(27) Percec, V.; Dulcey, A. E.; Peterca, M.; Ilies, M.; Sienkowska, M. J.; Heiney, P. A. Programming the Internal Structure and Stability of Helical Pores Self-Assembled from Dendritic Dipeptides via the Protective Groups of the Peptide. *J. Am. Chem. Soc.* **2005**, *127*, 17902−17909.